JOURNAL OF AIRCRAFT
Vol. 42, No. 1, January–February 2005

Time-Dependent Coefficient Reduced-Order Model for Unsteady Aerodynamics of Proprotors

M. Gennaretti* and L. Greco†
University of Rome, 00146 Rome, Italy

This work presents a methodology for the identification of a periodic-coefficient reduced-order model (ROM) for the prediction of perturbation aerodynamic loads on tiltrotor propellers in cruise flight. Although the result is a periodic-coefficient model, the process requires only frequency-domain aerodynamic solutions. Assuming the unperturbed proprotor in axial flow, the matrix that collects the aerodynamic transfer functions between blade perturbative boundary conditions and generalized aerodynamic forces is first derived. Then its rational matrix approximation, followed by combination with the equations describing the wing/pylon/proprotor kinetic coupling, yields the aerodynamic ROM. This ROM is expressed in terms of a set of linear equations that relate the time evolution of the aerodynamic loads acting on the proprotor blades to wing/pylon and deformable-blade degrees of freedom. Numerical results concerning a three-bladed proprotor connected to a bending and twisting wing will show that the unsteady aerodynamic loads predicted by the proposed ROM are in excellent agreement with those obtained through direct time-marching aerodynamic solutions.

Introduction

THE aim of the present paper is the identification of a periodic-coefficient reduced-order model (ROM) for the prediction of unsteady aerodynamic loads on tiltrotor propellers (proprotors) in axial motion. It is a state-space model that is based on an approximation of a frequency-domain aerodynamic solution and relates perturbations to the wing/pylon/proprotor motion with blade-generalized aerodynamic forces. (Gust perturbations might also be included.) When combined with the structural modeling, this state-space model yields a simple mathematical description of the wing/pylon/proprotor system that is very well suited for control applications and would be useful in other applications that need accurate prediction tools at low computational costs (e.g., preliminary design).

The development of simulation tools for the aeroelastic analysis of tiltrotors has captured the attention of many researchers. From the pioneering work of Ref. 1, many examples of tiltrotor aeroelastic modeling have been developed. Among these, we cite those presented in Refs. 2–6, where the model evolution is aimed at the accomplishment of parametric studies addressing the enhancement of the aeroelastic behavior of tiltrotors. However, aeroelastic models specifically focused on pylon/proprotor whirl-flutter analysis have also been developed. A review of them is given in Ref. 7, along with the outline of one specific model, whereas an example of whirl-flutter aeroservoelastic modeling is presented in Ref. 8.

Tiltrotor aeroelasticity is a very complex phenomenon wherein a strong interaction between wing and proprotor occurs both in terms of kinetic coupling and in terms of aerodynamic interference. It follows that the use of a direct computational fluid dynamics simulation for the evaluation of the aerodynamic loads acting on a wing-proprotor system requires a considerable computational effort. Hence, from the aerodynamic point of view, simplified (and as accurate as possible) models are highly desirable, especially for the purposes of design and control-law synthesis. Nonetheless, most of the work in the field of tiltrotor aeroelasticity is focused on the development of structural models as demonstrated in Refs. 1–6, where the aerodynamic loads are predicted by very simple two-dimensional, quasi-steady models combined with the strip-theory approach. Finite state aerodynamic models for rotary wings have been developed by Peters and his coworkers.[9,10] These models take into account the unsteady wake effects on the blade aerodynamics by considering a dynamic inflow, which in turn is related to the aerodynamic load acting on the rotor blades. (They can be treated as closed-loop approaches.[9]) They have been applied for helicopter rotor aeroelasticity, whereas a specific tiltrotor application is analyzed in Ref. 11, where the finite state modeling is focused on wing aerodynamics.

The approximate aerodynamic model presented here for describing unsteady forces on proprotor blades is based on a three-dimensional unsteady aerodynamic solution. The motion of the proprotor is assumed to be affected by that of the wing, through the pylon transmission. As mentioned earlier, a second wing–proprotor interaction effect is the aerodynamic interference. This is an important phenomenon that, even in the absence of perturbations, generates unsteady loads on the blades. Its inclusion would require the use of a time-domain free-wake aerodynamic solver (to take into account the distortion of the proprotor wake caused by the wing presence) and the adoption of a nonlinear ROM for the mathematical description of the blade loads. However, because we focus our attention on the identification of a particularly simplified prediction tool suited for control and preliminary design applications, in this work the wing–proprotor aerodynamic interference has been neglected. Specifically, considering the proprotor in axial flow (i.e., the case of a tiltrotor in airplane mode), our goal is the identification of a ROM describing the unsteady aerodynamic forces induced by motion perturbations caused by the proprotor–wing kinetic coupling and blade flexibility. This model consists of a set of linear equations that relate the time evolution of the aerodynamic loads acting on the proprotor blades to the wing perturbations and to the deformable-blade degrees of freedom (along with their first and second time derivatives). Because of the kinetic coupling between these perturbations and rotary motion of the blades, the equations have time-periodic coefficients. In addition, the inclusion of the flow memory effects produced by the proprotor wake vorticity yields the introduction of a finite number of additional aerodynamic states in the mathematical model.

In this work the novelty is that, although the ROM coefficients to be determined are periodic in time, the procedure proposed for their identification is based on a frequency-domain aerodynamic solution for the perturbed proprotor, followed by a rational matrix approximation of the resulting aerodynamic transfer-function matrix. Here, the frequency-domain solution is obtained by applying

Received 27 August 2003; revision received 15 December 2003; accepted for publication 17 December 2003.

*Associate Professor, Dipartimento di Ingegneria Meccanica e Industriale, via della Vasca Navale, 79; m.gennaretti@uniroma3.it.

†Graduate Engineer, Dipartimento di Ingegneria Meccanica e Industriale, via della Vasca Navale, 79.

the boundary element method (BEM) for three-dimensional, unsteady potential flows presented in Ref. 12, that has already been validated both for hovering and advancing rotor configurations (see also Ref. 13). However, the identification procedure proposed is applicable for whatever frequency-domain methodology is used for the aerodynamic solution. For instance, in this paper the analysis is performed for incompressible flows, but the procedure is identically applicable for compressible flows once the BEM aerodynamic solver is properly enhanced.

To the authors' knowledge the technique proposed in this paper is the only one available that yields the identification of a periodic-coefficient aerodynamic model starting from frequency-domain solutions. It may be considered an extension of the rational matrix finite state aerodynamics methodologies discussed in Refs. 14–18 for wing and hovering rotor aeroelastic applications. (An application for acoustoelasticity of fuselages is also presented in Ref. 19.) The extension is valid for those aerodynamic configurations where the periodicity of the ROM coefficients arises from coupling of the kinetic degrees of freedom of the system (and not from time variation of the relative position between body and wake vorticity). Note that the rapidity of the identification process depends on the type of frequency-domain solver available, whereas its accuracy is strictly related to the quality of rational approximations applied in the procedure.

Details of the procedure followed for the identification of the periodic-coefficient ROM are given in the next section for the case of rigid-blade proprotors. The extension to flexible-blade proprotor configurations is examined later. Finally, to assess the accuracy of the reduced-order aerodynamic model presented, the results of a numerical investigation will be presented. For a three-bladed proprotor connected to a bending and twisting wing, these concern the comparison between the aerodynamic loads predicted by the aerodynamic ROM and the aerodynamic loads obtained through direct time-marching aerodynamic (exact) solutions.

Rigid-Blade Prop-Rotor/Pylon System

Here we outline the methodology proposed for the identification of a linear, periodic-coefficient ROM describing the unsteady aerodynamic forces arising on the proprotor blades of a tiltrotor when perturbed from airplane-mode cruise flight. In this analysis, the complex aerodynamic interaction between proprotor wake and tiltrotor wing is neglected along with transonic and viscous effects, for which a nonlinear mathematical model would be necessary for an accurate description. We consider the general problem of an isolated pylon–proprotor system in axial motion in a potential flow. The motion perturbations are assumed to be caused by pylon vibrations about its uniform cruise translation and can be considered representative of the motion of the wing section to which the pylon–proprotor system would be connected in a realistic tiltrotor configuration. In this section the proprotor blades are assumed to be rigid.

The proposed procedure starts from the observation that, in potential flows, aerodynamic forces are generated by nonzero surface normal components of the body velocity. For the configurations of interest in this work, this is demonstrated in the Appendix through the application of a BEM approach. Indeed, it is shown that a set of N_f generalized aerodynamic blade forces induced by perturbations to a reference steady-state configuration (e.g., the cruise axial motion of a proprotor) may be expressed through a frequency-domain relationship of the following type:

$$\tilde{\underline{f}} = \underline{Q}(s)\,\tilde{\underline{\chi}} \tag{1}$$

where $\tilde{(\cdot)}$ denotes Laplace transformation, and $\underline{Q}(s)$ is the $[N_f \times N_c]$ matrix that collects the transfer functions relating the perturbative body-velocity normal components, $\underline{\chi}$, at the N_c BEM collocation points, to the aerodynamic forces $\underline{f}$ (see Appendix).

To derive a convenient expression for the body-velocity normal components we observe that, in a frame of reference fixed with the unperturbed flow, a general rigid-body motion of proprotor blades may be expressed by

$$\boldsymbol{v}(\boldsymbol{x}, t) = \boldsymbol{v}_H(t) + \boldsymbol{\omega}(t) \times (\boldsymbol{x} - \boldsymbol{x}_H) \tag{2}$$

where $\boldsymbol{v}_H$ is the hub velocity, $(\boldsymbol{x} - \boldsymbol{x}_H)$ is the distance vector between the hub and an arbitrary blade point $\boldsymbol{x}$, whereas $\boldsymbol{\omega}$ is the angular velocity of the blades. Introducing a frame of reference $Hxyz$ rigidly connected to the rotor blades, centered at the rotor hub, and with unit vectors $\boldsymbol{i}_r, \boldsymbol{j}_r, \boldsymbol{k}_r$, the velocity distribution in Eq. (2) may be expressed through a linear combination of six time-independent vector spatial distributions $\boldsymbol{\Psi}_n$ with coefficients corresponding to the scalar components of $\boldsymbol{v}_H$ and $\boldsymbol{\omega}$. Indeed, for $\boldsymbol{v}_H = v_H^x \boldsymbol{i}_r + v_H^y \boldsymbol{j}_r + v_H^z \boldsymbol{k}_r$ and $\boldsymbol{\omega} = \omega^x \boldsymbol{i}_r + \omega^y \boldsymbol{j}_r + \omega^z \boldsymbol{k}_r$, Eq. (2) may be recast in the following way:

$$\boldsymbol{v}(\boldsymbol{x}, t) = \sum_{n=1}^{6} v_n(t)\,\boldsymbol{\Psi}_n(\boldsymbol{x}) \tag{3}$$

where the generalized velocity components are defined as $v_1 = v_H^x$, $v_2 = v_H^y$, $v_3 = v_H^z$, $v_4 = \omega^x$, $v_5 = \omega^y$, and $v_6 = \omega^z$, whereas, for $\boldsymbol{x} - \boldsymbol{x}_H = (x - x_H)\boldsymbol{i}_r + (y - y_H)\boldsymbol{j}_r + (z - z_H)\boldsymbol{k}_r$, the vector spatial distributions are given by $\boldsymbol{\Psi}_1(\boldsymbol{x}) = \boldsymbol{i}_r$, $\boldsymbol{\Psi}_2(\boldsymbol{x}) = \boldsymbol{j}_r$, $\boldsymbol{\Psi}_3(\boldsymbol{x}) = \boldsymbol{k}_r$ and

$$\boldsymbol{\Psi}_4(\boldsymbol{x}) = -(z - z_H)\boldsymbol{j}_r + (y - y_H)\boldsymbol{k}_r$$

$$\boldsymbol{\Psi}_5(\boldsymbol{x}) = (z - z_H)\boldsymbol{i}_r - (x - x_H)\boldsymbol{k}_r$$

$$\boldsymbol{\Psi}_6(\boldsymbol{x}) = -(y - y_H)\boldsymbol{i}_r + (x - x_H)\boldsymbol{j}_r$$

Next we note that, 1) through the kinetic relationship between pylon motion and rotor rigid-body motion, for any given perturbation of the pylon motion it is possible to determine the corresponding generalized rotor velocities v_n defined earlier and, as a consequence, 2) if the transfer functions relating v_n and forces are known, forces induced by any pylon perturbation also may be determined. Therefore, in Eq. (1) it is convenient to replace the input column matrix $\underline{\chi}$ with its (time-independent) expression given in terms of the rotor generalized velocities v_n. For χ_m denoting the body-velocity normal component at the collocation point located at $\boldsymbol{x}_m$, we have (see Appendix)

$$\chi_m(t) = \boldsymbol{v}(\boldsymbol{x}_m, t) \cdot \boldsymbol{n}(\boldsymbol{x}_m) = \sum_{n=1}^{6} v_n(t)\,\boldsymbol{\Psi}_n(\boldsymbol{x}_m) \cdot \boldsymbol{n}(\boldsymbol{x}_m) \tag{4}$$

where $\boldsymbol{n}(\boldsymbol{x}_m)$ is the unit vector normal to the blade surface at the point $\boldsymbol{x}_m$. Transforming Eq. (4) into frequency domain and applying this process to boundary conditions at each collocation point yields the following matrix expression:

$$\tilde{\underline{\chi}} = \underline{E}^{\mathrm{BC}}\,\tilde{\underline{v}} \tag{5}$$

where $\underline{v}$ is the six-element column matrix collecting the generalized velocities v_n, whereas the entries of the $[N_c \times 6]$ boundary-condition matrix $\underline{E}^{\mathrm{BC}}$ are given by

$$E^{\mathrm{BC}}_{mn} = \boldsymbol{\Psi}_n(\boldsymbol{x}_m) \cdot \boldsymbol{n}(\boldsymbol{x}_m) \tag{6}$$

Combining Eq. (1) with Eq. (5) yields

$$\tilde{\underline{f}} = \underline{E}(s)\,\tilde{\underline{v}} \tag{7}$$

where $\underline{E}(s) = \underline{Q}(s)\,\underline{E}^{\mathrm{BC}}$ is the $[N_f \times 6]$ aerodynamic transfer-function matrix that relates the generalized rigid-rotor velocities to the corresponding aerodynamic forces.

Finite-State Approximation

The entries of matrix $\underline{Q}$ (and of matrix $\underline{E}$, as well) are transcendental functions of the Laplace variable s because of the time-delay terms appearing in the aerodynamic solution from wake-vorticity convection (see Appendix). An aerodynamic operator of this type would give rise to an infinite-dimension state-space problem in the time domain. Thus, to identify the aerodynamic ROM, this difficulty is overcome by utilizing rational expressions for approximating the transfer functions in the aerodynamic matrix. Techniques of this type are frequently used for the aeroelastic analysis of fixed wings[14,17] and have already been applied for the stability analysis of hovering

rotors.[18] The specific approach used here follows the methodology presented in Ref. 16 and is closely related to the well-known minimum-state technique introduced by Karpel[14] (see Refs. 16 and 19 for a discussion of this issue). Then, applying this methodology, the following approximate rational-matrix expression is derived for the aerodynamic transfer-function matrix:

$$\underline{E}(s) \approx s\,\underline{A}_1 + \underline{A}_0 + \underline{C}[s\underline{I} - \underline{A}]^{-1}\underline{B} \tag{8}$$

where $\underline{A}_1$, $\underline{A}_0$, $\underline{A}$, $\underline{B}$, and $\underline{C}$ are real, fully populated matrices (see also Ref. 16). Matrices $\underline{A}_1$ and $\underline{A}_0$ have dimensions $[N_f \times 6]$, $\underline{A}$ is a $[N_a \times N_a]$ matrix containing the N_a poles included in the approximating expression, $\underline{C}$ is a $[N_f \times N_a]$ matrix, and $\underline{B}$ has dimensions $[N_a \times 6]$. In the preceding expression, the first-order polynomial truncation is suggested by the fact that the asymptotic behavior of transfer functions between velocities and aerodynamic forces is linear, as induced by the presence of the first time derivative of the velocity potential in the Bernoulli theorem (see matrix $\underline{E}_p$ in the Appendix) together with the time independence of the boundary-condition matrix $\underline{E}^{\mathrm{BC}}$.

Next, combining Eq. (8) with Eq. (7) and transforming into a time domain yields the following constant-coefficient expression relating the generalized rigid-blade velocities (and their first time derivatives) with the corresponding unsteady aerodynamic forces arising on the perturbed blades:

$$\underline{f}(t) = \underline{A}_1\dot{\underline{v}} + \underline{A}_0\underline{v} + \underline{C}\underline{r} \tag{9}$$

$$\dot{\underline{r}} = \underline{A}\underline{r} + \underline{B}\underline{v} \tag{10}$$

where $\underline{r}$ is the column matrix that collects the N_a additional aerodynamic states associated to the poles included in the approximating aerodynamic matrix, a consequence of the flow memory effects included in matrix $\underline{E}(s)$.

Pylon/Blade Kinetic Coupling and ROM Identification

The last step in the procedure for the identification of the proprotor aerodynamic ROM is the replacement, in Eqs. (9) and (10), of the generalized rigid-blade velocities with the kinetic equations that relate them to the pylon degrees of freedom (or to the gust velocity, if present). Introducing a frame of reference $O_p x_p y_p z_p$ rigidly connected with the pylon, the six degrees of freedom of the perturbative pylon rigid-body motion can be defined by the small displacements u_x, u_y, u_z of the origin O_p along the three axes, together with the small rotations $\alpha_x, \alpha_y, \alpha_z$ of the frame about the same axes. (Note that, for a wing–proprotor configuration with the pylon rigidly fixed to the wing they represent the degrees of freedom of the wing section where the pylon/proprotor system is connected.) Combining the pylon motion with the helicoidal cruise-state motion defined by the translation velocity $\boldsymbol{V}$ along the unperturbed rotor shaft and the rotational velocity $\boldsymbol{\Omega}$ about the same axis, in Eq. (2) we have

$$\boldsymbol{v}_H(t) = \boldsymbol{V} + \boldsymbol{v}_H^{\mathrm{per}} \qquad \text{and} \qquad \boldsymbol{\omega}(t) = \boldsymbol{\Omega} + \boldsymbol{\omega}^{\mathrm{per}}$$

where $\boldsymbol{v}_H^{\mathrm{per}} = \boldsymbol{v}_H^{\mathrm{per}}(u_x, u_y, u_z, \alpha_x, \alpha_y, \alpha_z)$ and $\boldsymbol{\omega}^{\mathrm{per}} = \boldsymbol{\omega}^{\mathrm{per}}(\alpha_x, \alpha_y, \alpha_z)$ denote, respectively, the hub velocity and the rotor angular velocity caused by the perturbative pylon motion. Then, determining the rotor-frame components of vectors $\boldsymbol{v}_H$ and $\boldsymbol{\omega}$ and limiting our analysis to first-order perturbation terms, the following relationship between generalized rigid-blade velocities and pylon degrees of freedom can be determined:

$$\underline{v}(t) = \underline{K}_1(\Omega, t)\dot{\underline{q}}^p + \underline{K}_0(V, \Omega, t)\underline{q}^p \tag{11}$$

where $\underline{q}^p = \{u_x\ u_y\ u_z\ \alpha_x\ \alpha_y\ \alpha_z\}^T$, whereas $\underline{K}_1$ and $\underline{K}_0$ are $[6 \times 6]$ time-periodic kinetic matrices. (A periodic-coefficient relationship between $\underline{v}$ and gust velocity can also be determined for gust-perturbed tiltrotor configurations.) Note that the time dependence of the kinetic matrices is caused by the relative motion between the rotating rotor hub frame of reference $Hxyz$ (where the scalar components of the rotor velocity are defined) and the nonrotating pylon frame of reference $O_p x_p y_p z_p$ (where the pylon perturbations are defined). In addition, the dependence of $\underline{K}_0$ on V describes the time variation of the components of the translation velocity in the rotor-hub frame, which are caused by the pylon-frame perturbative rotations. To explain this, let us assume that the hub-frame axis z and the pylon-frame axis z_p are both aligned along the rotor shaft and that initially the rotor axes x and y are parallel to the pylon axes x_p and y_p, respectively. Then, consider the pylon perturbations u_x (translation) and α_x (rotation). We observe that u_x induces a perturbative velocity $\dot{u}_x$ parallel to the x_p pylon axis; in the (rotating) rotor hub frame it has the following two components:

$$v_1 = \dot{u}_x \cos(\Omega t), \qquad v_2 = -\dot{u}_x \sin(\Omega t) \tag{12}$$

In addition, the rotation of the pylon frame yields a $V\alpha_x$ perturbation velocity along the pylon y_p axis which, in the rotor frame, has components

$$v_1 = V\alpha_x \sin(\Omega t), \qquad v_2 = V\alpha_x \cos(\Omega t) \tag{13}$$

Hence, Eq. (12) is an example of time-periodic entries of matrix $\underline{K}_1$, whereas examples of time-periodic entries of matrix $\underline{K}_0$ depending on the flight velocity V are given in Eq. (13). Note that the advantage in defining the boundary conditions $\underline{\chi}$ in terms of the generalized velocities $\underline{v}$, rather than directly in terms of the pylon degrees of freedom $\underline{q}^p$, is that constant-coefficient relationships are involved. When transformed into the frequency domain, they yield the simple transfer function between $\underline{v}$ and $\underline{\chi}$ given in Eq. (5). On the contrary, Eq. (11) shows that expressing $\underline{\chi}$ directly in terms of $\underline{q}^p$ would give rise to time-periodic coefficient relationships. In turn, in the frequency domain these would produce complex convolution integral terms, and the rational matrix approximation would no longer be applicable to the resulting $\underline{E}$. In that case, the alternative to get a finite state model could be the application of the rational matrix approximation to $\underline{Q}$ [see Eq. (1)], with the drawback of requiring the approximation of a number of entries much higher than those appearing in $\underline{E}$. (Hundreds of collocation points might be introduced by the application of the BEM approach.)

Finally, the identification of the proprotor aerodynamic ROM is obtained by combining Eqs. (9) and (10) with Eq. (11). This yields the following set of equations:

$$\underline{f}(t) = \underline{D}_2(t)\ddot{\underline{q}}^p + \underline{D}_1(t)\dot{\underline{q}}^p + \underline{D}_0(t)\underline{q}^p + \underline{C}\underline{r}$$

$$\dot{\underline{r}} = \underline{A}\underline{r} + \underline{H}_1(t)\dot{\underline{q}}^p + \underline{H}_0(t)\underline{q}^p$$

where

$$\underline{D}_2(t) = \underline{A}_1\underline{K}_1(t)$$

$$\underline{D}_1(t) = \underline{A}_1[\dot{\underline{K}}_1(t) + \underline{K}_0(t)] + \underline{A}_0\underline{K}_1(t)$$

$$\underline{D}_0(t) = \underline{A}_1\dot{\underline{K}}_0(t) + \underline{A}_0\underline{K}_0(t)$$

$$\underline{H}_1(t) = \underline{B}\underline{K}_1(t), \qquad \underline{H}_0(t) = \underline{B}\underline{K}_0(t)$$

are periodic matrices. For a given time evolution of the pylon perturbative motion variables $\underline{q}^p$, the preceding equations yield the corresponding aerodynamics forces $\underline{f}$ acting on the blades of the proprotor.

Deformable-Blade Prop-Rotor/Pylon System

In this section, we extend the aforementioned methodology to deformable-blade configurations. In the case of deforming proprotor blades, some additional terms appear in the aerodynamic ROM. These arise from the contribution of blade deflections to the boundary conditions and imply the inclusion of the degrees of freedom associated with the blade deformation among the perturbation variables.

The effect of blade flexibility on aerodynamic loads is twofold: 1) elastic vibrations yield an additional term, $\boldsymbol{v}^d$, in the velocity distribution of Eq. (2) that becomes

$$\boldsymbol{v}(\boldsymbol{x}, t) = \boldsymbol{v}_H(t) + \boldsymbol{\omega}(t) \times (\boldsymbol{x} - \boldsymbol{x}_H) + \boldsymbol{v}^d(\boldsymbol{x}, t) \tag{14}$$

and 2) elastic deformation causes rotation of the unit normal vectors $\boldsymbol{n}$ appearing in the evaluation of the boundary conditions. To include these contributions into the aerodynamic ROM, for each proprotor blade, it is convenient to express the displacement caused by elastic deformation, $\boldsymbol{d}^d(\boldsymbol{x}, t)$, in terms of the following combination of N_m shape functions:

$$\boldsymbol{d}^d(\boldsymbol{x}, t) = \sum_{l=1}^{N_m} q_l^d(t)\boldsymbol{\Phi}_l(\boldsymbol{x}) \tag{15}$$

where the scalars q_l^d are the generalized coordinates of the blade elastic motion, whereas the vectors $\boldsymbol{\Phi}_l$ are shape functions chosen for the description of the deformation distribution, which have time-independent components in the $Hxyz$ rotor hub frame. Using Eq. (15), the blade velocity induced by elastic vibration is given by

$$\boldsymbol{v}^d(\boldsymbol{x}, t) = \sum_{l=1}^{N_m} \dot{q}_l^d(t)\boldsymbol{\Phi}_l(\boldsymbol{x}) \tag{16}$$

whereas the unit normals on the deformed-blade surface can be expressed using the following first-order truncation of the Taylor series in terms of the generalized coordinates; that is,

$$\boldsymbol{n}(\boldsymbol{x}, t) = \boldsymbol{n}_{\text{rig}}(\boldsymbol{x}) + \sum_{l=1}^{N_m} \frac{\partial \boldsymbol{n}(\boldsymbol{x})}{\partial q_l^d} q_l^d(t) \tag{17}$$

where $\boldsymbol{n}_{\text{rig}}$ denotes a normal vector in the rigid-blade configuration, and $\partial \boldsymbol{n}/\partial q_l^d$ are vectors with time-constant rotor-frame components [that can be evaluated through Eq. (15)]. Combining Eqs. (16) and (17) with Eq. (14), under the assumption of linear analysis, the perturbation boundary conditions at each blade of the proprotor are given by

$$\chi_m(t) = \boldsymbol{v}(\boldsymbol{x}_m, t)\cdot\boldsymbol{n}(\boldsymbol{x}_m) = \sum_{n=1}^{6} v_n(t)\boldsymbol{\Psi}_n(\boldsymbol{x}_m)\cdot\boldsymbol{n}_{\text{rig}}(\boldsymbol{x}_m)$$

$$+ \sum_{l=1}^{N_m} \dot{q}_l^d(t)\boldsymbol{\Phi}_l(\boldsymbol{x}_m)\cdot\boldsymbol{n}_{\text{rig}}(\boldsymbol{x}_m) + \sum_{l=1}^{N_m} \boldsymbol{v}_{\text{cr}}\cdot\frac{\partial \boldsymbol{n}(\boldsymbol{x}_m)}{\partial q_l^d} q_l^d(t) \tag{18}$$

where $\boldsymbol{v}_{\text{cr}} = \boldsymbol{V} + \boldsymbol{\Omega}\times(\boldsymbol{x}-\boldsymbol{x}_H)$ is the unperturbed proprotor cruise velocity. Transforming Eq. (18) into the frequency domain and repeating this procedure at each control point and for all of the N_b blades of the proprotor, the following matrix expression is obtained:

$$\tilde{\underline{\chi}} = \underline{E}_{\text{rig}}^{\text{BC}}\,\tilde{\underline{v}} + \underline{E}_{\text{def}}^{\text{BC}}(s)\tilde{\underline{q}}^d \tag{19}$$

where $\underline{q}^d$ is the column matrix collecting the $N_b * N_m$ generalized coordinates, q_l^d, of the elastic motion of all of the rotor blades, and $\underline{E}_{\text{rig}}^{\text{BC}}$ coincides with the matrix defined in Eq. (6), whereas the entries of the $[N_c \times N_b * N_m]$ matrix $\underline{E}_{\text{def}}^{\text{BC}}$ are given by

$$E_{\text{def}}^{\text{BC}}(s)_{ml} = \boldsymbol{v}_{\text{cr}}(\boldsymbol{x}_m)\cdot\frac{\partial \boldsymbol{n}(\boldsymbol{x}_m)}{\partial q_l^d} + s\boldsymbol{\Phi}_l(\boldsymbol{x}_m)\cdot\boldsymbol{n}_{\text{rig}}(\boldsymbol{x}_m)$$

Introducing the $(6 + N_b * N_m)$-element column matrix

$$\underline{w} = \begin{Bmatrix} \underline{v} \\ \underline{q}^d \end{Bmatrix}$$

which collects the rotor generalized velocities and blade-deformation coordinates, along with the $[N_c \times (6 + N_b * N_m)]$ boundary-condition matrix $\underline{E}^{\text{BC}}(s) = [\underline{E}_{\text{rig}}^{\text{BC}} \;\; \underline{E}_{\text{def}}^{\text{BC}}(s)]$, and combining Eq. (1) with Eq. (2) yields

$$\underline{\tilde{f}} = \underline{E}(s)\,\tilde{\underline{w}} \tag{20}$$

where $\underline{E}(s) = \underline{Q}(s)\underline{E}^{\text{BC}}(s)$ is the $[N_f \times (6 + N_b * N_m)]$ aerodynamic transfer-function matrix that relates generalized coordinates of blade elastic motion and rigid-body rotor velocities to the corresponding aerodynamic forces.

Akin to the rigid-blade case, to determine the aerodynamic finite state model, this matrix is approximated through a rational-matrix expression. Following again the methodology of Ref. 16 we have

$$\underline{E}(s) \approx s^2\underline{A}_2 + s\underline{A}_1 + \underline{A}_0 + \underline{C}\left[s\underline{I} - \underline{A}\right]^{-1}\underline{B} \tag{21}$$

where matrices $\underline{A}_2$, $\underline{A}_1$, and $\underline{A}_0$ have dimensions $[N_f \times (6 + N_b * N_m)]$ and may be conveniently partitioned in the following way: $\underline{A}_k = [\underline{A}_k^v \;\; \underline{A}_k^q]$ (with $\underline{A}_2^v = 0$). In addition, $\underline{A}$ is a square matrix with dimensions $[N_a \times N_a]$, $\underline{C}$ is a $[N_f \times N_a]$ matrix, and $\underline{B}$ has dimensions $[N_a \times (6 + N_b * N_m)]$ and may be partitioned as $\underline{B} = [\underline{B}^v \;\; \underline{B}^q]$. With respect to the rigid-blade case, here the $\underline{A}_2$ matrix term has been added because of the fact that $\underline{E}^{\text{BC}}$ is linearly dependent on s, as caused by the presence of the variables associated to the elastic deformation. (It is possible to show that the asymptotic behavior of transfer functions between displacements and aerodynamic forces is quadratic; see, e.g., Ref. 19.)

ROM Identification

Finally, the deformable proprotor aerodynamic ROM is derived by combining Eq. (21) with Eq. (20), transforming into the time domain, and then expressing the generalized rotor rigid-body velocities $\boldsymbol{v}$ in terms of the pylon degrees of freedom [Eq. (11)]. This process yields the following set of equations for the perturbation unsteady aerodynamic forces,

$$\underline{f}(t) = \underline{D}_2(t)\ddot{\underline{q}} + \underline{D}_1(t)\dot{\underline{q}} + \underline{D}_0(t)\underline{q} + \underline{C}\underline{r} \tag{22}$$

$$\dot{\underline{r}} = \underline{A}\underline{r} + \underline{H}_1(t)\dot{\underline{q}} + \underline{H}_0(t)\underline{q} \tag{23}$$

where the $(6 + N_b * N_m)$-element column matrix of the input variables is defined as

$$\underline{q} = \begin{Bmatrix} \underline{q}^p \\ \underline{q}^d \end{Bmatrix}$$

and the periodic matrices appearing in Eqs. (22) and (23) are defined through the following partitions: $\underline{D}_j(t) = [\underline{D}_j^p(t) \;\; \underline{D}_j^d(t)]$ and $\underline{H}_j(t) = [\underline{H}_j^p(t) \;\; \underline{H}_j^d(t)]$, with

$$\underline{D}_2^p(t) = \underline{A}_1^v\underline{K}_1(t), \qquad \underline{D}_2^d(t) = \underline{A}_2^q$$

$$\underline{D}_1^p(t) = \underline{A}_1^v[\dot{\underline{K}}_1(t) + \underline{K}_0(t)] + \underline{A}_0^v\underline{K}_1(t), \qquad \underline{D}_1^d(t) = \underline{A}_1^q$$

$$\underline{D}_0^p(t) = \underline{A}_1^v\dot{\underline{K}}_0(t) + \underline{A}_0^v\underline{K}_0(t), \qquad \underline{D}_0^d(t) = \underline{A}_0^q$$

$$\underline{H}_1^p(t) = \underline{B}^v\underline{K}_1(t), \qquad \underline{H}_1^d(t) = 0$$

$$\underline{H}_0^p(t) = \underline{B}^v\underline{K}_0(t), \qquad \underline{H}_0^d(t) = \underline{B}^q$$

For a given time evolution of the pylon degrees of freedom, $\underline{q}^p$, and of the generalized coordinates of the blade deformation $\underline{q}^d$, Eqs. (22) and (23) give the corresponding aerodynamics forces $\underline{f}$ acting on the blades of the proprotor.

Numerical Results

Numerical investigation has been performed to assess the accuracy of the ROM presented earlier in predicting the aerodynamic loads arising on a proprotor perturbed from airplane-mode flight conditions. A three-bladed proprotor with radius $R = 3.97$ m and cruise flight defined by axial velocity $V = 25.7$ m/s and rotor angular velocity $\Omega = 40.4$ rad/s has been examined. This is one of the cases analyzed in Ref. 1 and, in particular, is the one with the shortest wake pitch and, hence, the strongest wake vorticity effect on blade aerodynamics. Simplifying the geometric characteristics of the Boeing proprotor considered in Ref. 1, the blade collective-pitch angle has been assumed to vary linearly along the blade span from the root value $\theta_{\text{root}} = 38.15$ deg to the tip value $\theta_{\text{tip}} = 5.15$ deg (therefore yielding the same three-fourth span collective pitch used in Ref. 1), whereas the chord length has been assumed to be constant and equal to 0.478 m. Such a configuration corresponds to a spanwise distribution of the angle of attack that yields an almost

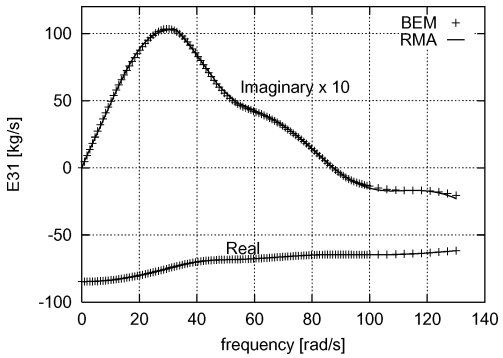

Fig. 1 RMA of transfer function between v_1 and lift on blade 1, using 30 poles.

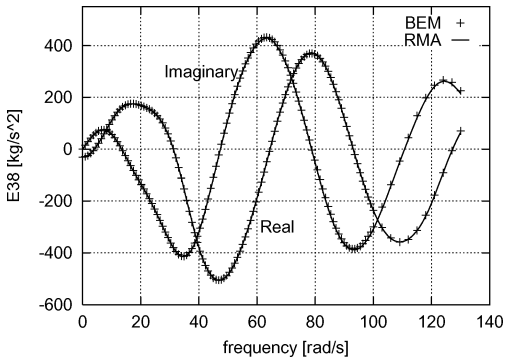

Fig. 2 RMA of transfer function between q_2^d and lift on blade 1, using 30 poles.

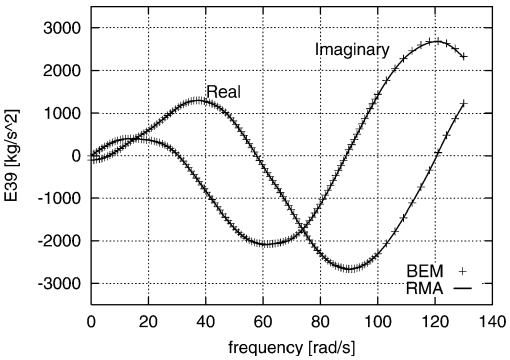

Fig. 3 RMA of transfer function between q_3^d and lift on blade 1, using 30 poles.

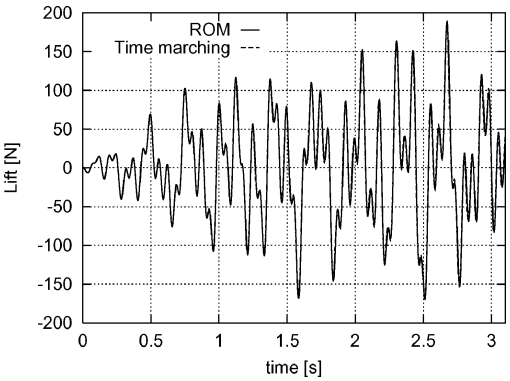

Fig. 4 Lift on blade 1 caused by wing/blade harmonic perturbations.

nonlifting condition and is the unperturbed proprotor trim state considered in the following results. [The reference condition chosen does not have influence on the validation of the methodology presented in that, for proprotors, its main effect is on the definition of the kinetic matrices in Eq. (11).] With the exception of one of the cases analyzed (for which a gimbaled rotor has been considered), the proprotor examined has been assumed to have hingeless elastic flap bending blades. For the bending deformation described through the first nonrotating beam bending mode, the proprotor perturbation motion is defined by nine degrees of freedom, that is, those related to the pylon motion $\underline{q}^p$ with the addition of three elastic degrees of freedom, $\underline{q}^d$ (one bending mode for each blade).

First, some results concerning the rational matrix approximation (RMA) of the aerodynamic matrix $\underline{E}(s)$ are shown [see Eqs. (8) and (21)]. For the hub frame of reference, $Hxyz$, with the z axis aligned with the rotor shaft and the y axis aligned with one of the rotor blades (blade 1), consider the transfer function $E_{31}(s)$ between the generalized velocity component v_1 and the lift force (proprotor thrust) acting on blade 1. Figure 1 shows the comparison between the values of this transfer function computed by the frequency-domain BEM approach outlined in the Appendix and those given by the RMA, with the introduction of 30 poles. In the frequency range examined, the agreement between the two curves proves that the accuracy of the RMA is excellent both for the real part and for the imaginary part of the transfer function. In addition, Figs. 2 and 3 show, respectively, the transfer functions, $E_{38}(s)$ and $E_{39}(s)$, relating lift on blade 1 to bending mode perturbations, q_2^d, q_3^d, on blades 2 and 3. (During rotation, blade 2 follows blade 1 and blade 3 follows blade 2.) Also in these cases, the agreement between the transfer functions calculated by the BEM and the transfer functions given by the RMA is excellent. Note that the wavy behavior in Figs. 2 and 3 is caused by the vorticity in the wakes of blades 2 and 3, respectively, which, for the low-advance-ratio case examined, are very close to the surface of blade 1. (Forces on blade 1 are influenced by perturbations to blades 2 and 3 mainly through the vorticity generated and convected along the wakes.) The capture of wavy functions is the origin of the high number of poles introduced in the matrix-fraction approximation. The same good accuracy may be observed for all of the transfer functions in matrix $\underline{E}$.

Then, starting from the rational approximation of the aerodynamic transfer functions and following the procedure outlined earlier, we have determined the aerodynamic ROM of the considered proprotor. To assess its accuracy for a realistic case, the pylon is been assumed to be fixed to the tip section of a tiltrotor wing subject to flapping, w, and torsional, ϑ, elastic motion. Combining this motion with the blade elastic deformations, it is possible to determine the variables to be used as input for the ROM presented in this paper and, thus, predict the aerodynamic loads associated with the considered perturbations. Two different motions are examined in this numerical investigation. [It is worth noting that the wing/pylon/proprotor motions chosen in this analysis are arbitrary and affect the definition of the kinetic matrices in Eq. (11) without altering the core of the methodology.] One is a combination of wing and blade deformations that, starting from rest conditions, asymptotically tend to a harmonic behavior. Specifically, the dynamics of the wing/pylon/proprotor system is described by the following functions for the first time derivative of wing-tip and blade degrees of freedom:

$$\dot{w}(t) = A_w(1 - e^{-\alpha_w t})\sin(\omega_w t) \tag{24}$$

$$\dot{\vartheta}(t) = A_\vartheta(1 - e^{-\alpha_\vartheta t})\sin(\omega_\vartheta t) \tag{25}$$

$$\dot{q}_j^d(t) = A_q(1 - e^{-\alpha_q t})\sin[\omega_q t - (j-1)(2\pi/3)]$$

for $j = 1, 2, 3$, with $A_w = 0.8$ m/s, $A_\vartheta = 0.17$ rad/s, $A_q = 0.27$ m/s, $\omega_w = \Omega/3$, $\omega_\vartheta = 1.5\Omega$, $\omega_q = 1.2\Omega$, and $\alpha_w = \alpha_\vartheta = \alpha_q = 1\ \text{s}^{-1}$. The aerodynamic forces associated with this motion have been evaluated both by applying the reduced-order aerodynamics presented in this work and through the time-marching (exact) solution of the time-domain version of the BEM approach outlined in the Appendix. Figure 4 depicts the lift force acting on blade 1 as computed by both approaches. The two curves are in excellent agreement and this shows that the aerodynamic loads predicted by the ROM are very

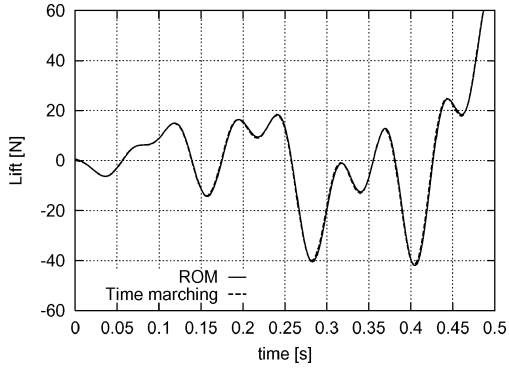

Fig. 5 Lift on blade 1 caused by wing/blade harmonic perturbations; details of the initial evolution.

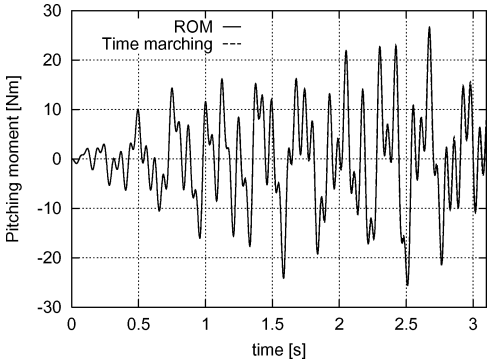

Fig. 6 Pitching moment on blade 1 caused by wing/blade harmonic perturbations.

accurate. This is confirmed in Fig. 5 where, changing the scales of the axes, a more detailed analysis of the comparison is shown for the initial evolution of the motion. The ROM shows the same excellent accuracy in predicting all of the aerodynamic loads examined. As a further example, in Fig. 6 the comparison between time-marching and ROM predictions is shown for the pitching moment on blade 1 about the midchord line. Also in this case, no difference between the two results can be observed and, hence, the high level of accuracy of ROM approximation is confirmed.

The second wing/pylon/proprotor perturbation motion that has been examined simulates damped oscillations of a stable wing perturbed from an equilibrium configuration. (The rotor blades are assumed to be rigid.) For this problem, in the absence of elastic degrees of freedom of the blades, the aerodynamic matrix $\underline{E}(s)$ is of reduced dimensions with respect to the previous case, and the same excellent accuracy of its RMA (e.g., Fig. 1) has been reobtained including only 20 poles. (Note that the transfer functions related to the pylon degrees of freedom have a less wavy behavior than those related to the blade elastic degrees of freedom.)

The wing motion considered is given by the following expressions:

$$w(t) = A_w e^{-\alpha_w t} \sin(\omega_w t), \qquad \vartheta(t) = A_\vartheta e^{-\alpha_\vartheta t} \sin(\omega_\vartheta t)$$

where $A_w = R/5$, $A_\vartheta = \pi/20$, $\alpha_w = 0.2\ \mathrm{s}^{-1}$, $\alpha_\vartheta = 0.4\ \mathrm{s}^{-1}$, and the values of ω_w and ω_ϑ are equal to those used in the analysis discussed earlier. Lift force on blade 1 caused by such perturbations is depicted in Fig. 7, both as predicted by the ROM approach and as computed through the BEM time-marching solution. Akin to the harmonic input case, for the damped motion the solution predicted by the ROM approach is also very accurate; this is confirmed by the detailed comparison in Fig. 8, where the force evolution is shown only in a limited time range. The same excellent agreement between ROM and time-marching solutions is observed also for all of the aerodynamic loads analyzed and, as an example, the comparison concerning the flapping moment on blade 1 is depicted in

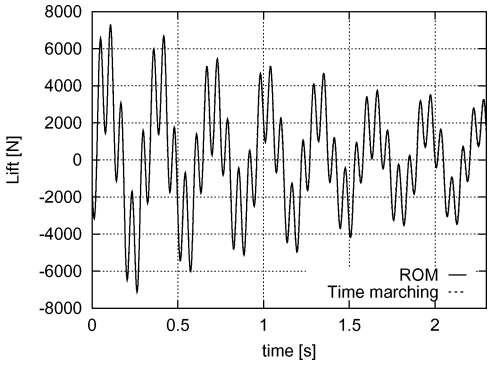

Fig. 7 Lift on blade 1 caused by wing-damped perturbations.

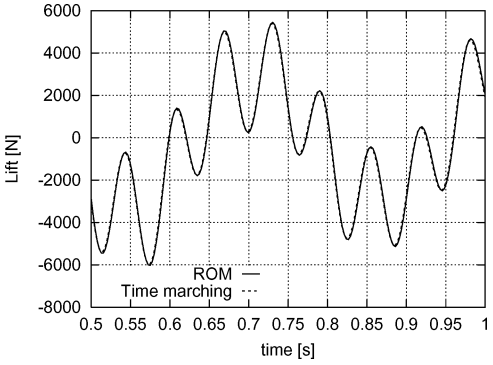

Fig. 8 Lift on blade 1 caused by wing-damped perturbations; details in a limited time range.

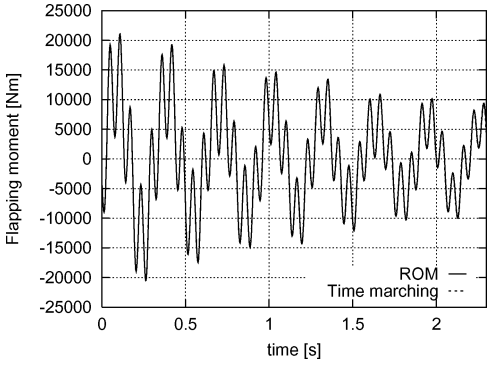

Fig. 9 Flapping moment on blade 1 caused by wing-damped perturbations.

Fig. 9. (This moment has been defined as the one about the root axis orthogonal to the midchord line, in the plane of rotation). Furthermore, Fig. 10 shows the ROM/time-marching comparison for the flapping moments acting on the three blades of the proprotor examined. For the sake of clarity, in this figure only a limited time range is considered, and the curves concerning blade 1 are identified by triangles, the curves concerning blade 2 are identified by squares, and the flapping moments on blade 3 are identified by circles. This figure demonstrates that the aerodynamic loads predicted by the applied ROM are very accurate for all of the blades of the examined proprotor. From this figure it is also possible to analyze the effect of the timing of the pylon motion with respect to blade position. In the case examined here, at $t = 0$ the wing is in its unperturbed configuration (i.e., $w = 0$ and $\vartheta = 0$), blade 1 is aligned with the wing in the outboard position, and blades 2 and 3 are correspondingly located with respect to the wing. These differences in pylon-motion/blade-position timing induce different loads on different blades because, at the same angular position, different blades experience different

Table 1 ROM accuracy index

Poles	Relative L_2 norm
5	0.122
8	0.100
12	0.031
20	0.018

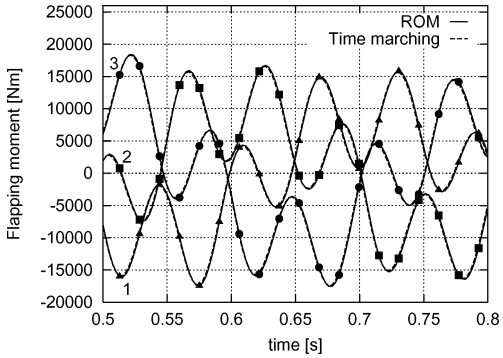

Fig. 10 Details of flapping moments on the blades caused by wing-damped perturbations.

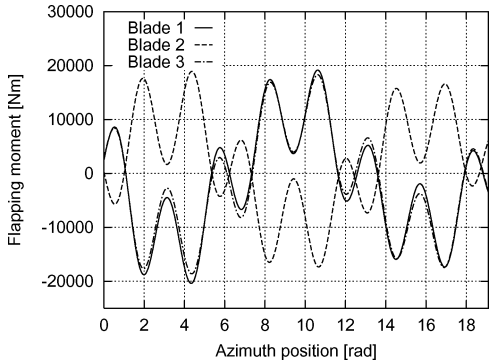

Fig. 11 Flapping moment on blades vs blade angular position. Flapping and twisting wing-damped perturbations.

motion perturbations. This is shown in Fig. 11, where each flapping moment computed by the ROM is plotted as a function of the azimuthal location of the corresponding blade. The load on blade 2 appears to be very different from that on blades 1 and 3. However, the similarity of the loads on blades 1 and 3 is a specific result of the examined motion. Indeed, if the twisting motion of the wing is neglected, the flapping moments on the three blades show three different evolutions, as depicted in Fig. 12, and prove the dependence of blade loads on pylon-motion/blade-position timing. Note that the periodicity shown by the blade loads has a period that depends on the relation between the frequency of the pylon motion and the angular velocity of the blade. (The period in Fig. 12 is larger than that in Fig. 11 because of the lack of the higher frequency wing twisting motion.)

For the damped wing/pylon perturbation motion, we have also examined the sensitivity of the ROM to the accuracy of the RMA. In particular, we have analyzed the effect of decreasing the number of additional aerodynamic states. (For the sake of simplicity of the aeroelastic model and reduction of computational costs, it is desirable to have as few additional aerodynamic states as possible.) As an index of accuracy we have considered (in the time interval $1\text{ s} \le t \le 2\text{ s}$) the L_2 norm of the difference between ROM and time-marching predictions of blade 1 lift divided by the root mean square of the same load given by the time-marching solution. (In the following, this parameter is referred to as "relative L_2 norm.") Table 1 shows the values of the relative L_2 norm that have been computed using different numbers of poles in the rational approximation of the aerodynamic transfer functions. As expected, the higher the number

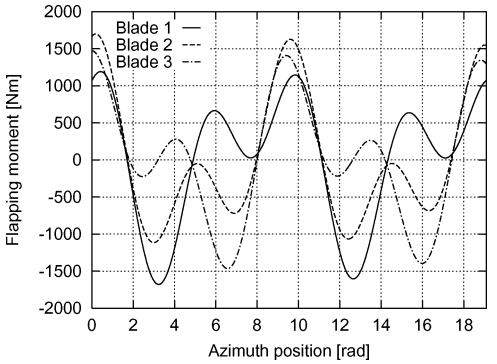

Fig. 12 Flapping moment on blades vs blade angular position. Flapping wing-damped perturbations.

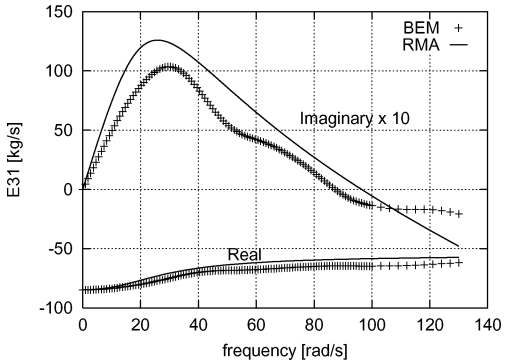

Fig. 13 RMA of transfer function between v_1 and lift force on blade 1, using five poles.

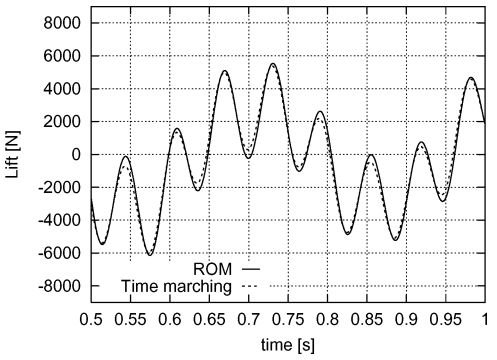

Fig. 14 Lift on blade 1 caused by wing-damped perturbations. ROM from five-pole RMA.

of additional aerodynamic states included, the higher the accuracy of the ROM solution. However, it is interesting to observe that the accuracy of the predictions given by the aerodynamic ROM remains satisfactory even for considerable reductions of the aerodynamic states. As an example, the following figures illustrate the solution obtained when including five poles. The comparison between data computed through the frequency-domain BEM and their rational approximation is shown in Fig. 13 for the transfer function relating the velocity component v_1 to the lift on blade 1. In this case some significant inaccuracies arise, but, in the examined, frequency range the overall behavior seems to be captured. The influence of these discrepancies on the loads predicted by the aerodynamic ROM is shown in Fig. 14, where details of ROM/time-marching comparison are depicted for lift on blade 1. As indicated by the relative L_2 norm in Table 1, despite the fact that only five aerodynamic states have been introduced, the loads predicted by the proposed aerodynamic ROM are in satisfactory agreement with those from the time-marching solution.

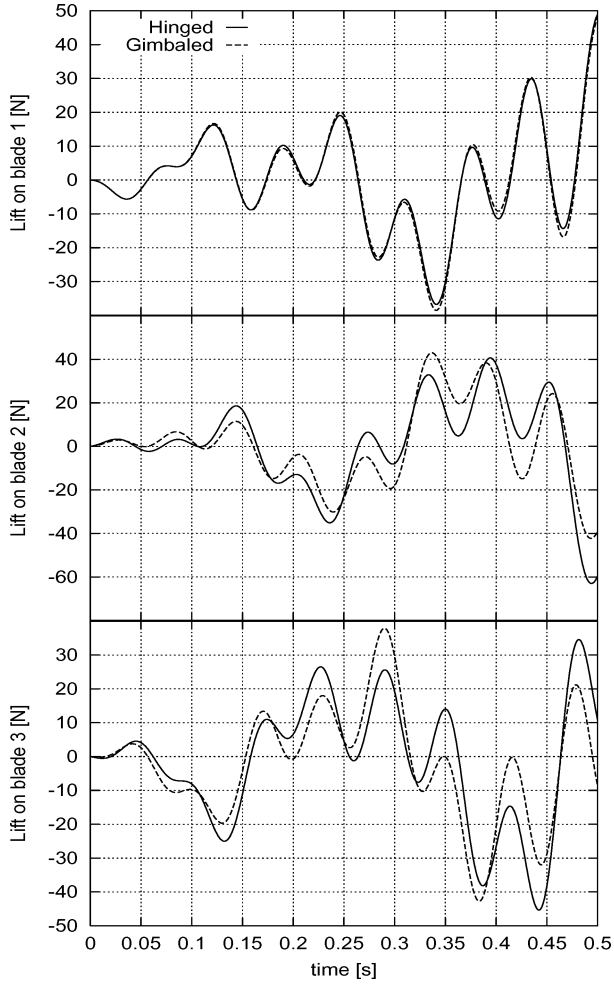

Fig. 15 Lift on blades 1, 2, and 3. Gimbaled proprotor vs hinged-blade proprotor.

Finally, in view of the fact that, in these days, many proprotors use gimbaled hubs, we have examined the difference between blade loads on a configuration of this type and those on one in which the blades are free to move independently of each other. The gimbaled rotor is assumed to have rigid blades with blade 1 flapping as described by

$$\dot{\beta}(t) = A_\beta(1 - e^{-\alpha_\beta t})\sin(\omega_\beta t)$$

with $A_\beta = 0.08$ rad/s, $\omega_\beta = 1.1\,\Omega$, $\alpha_\beta = 0.2$ s^{-1}, and blades 2 and 3 moving correspondingly. The proprotor used for comparison has been assumed to have three rigid blades, each flapping about a root hinge, defined by

$$\dot{\beta}_j(t) = A_\beta(1 - e^{-\alpha_\beta t})\sin[\omega_\beta t - (j-1)(2\pi/3)]$$

with $j = 1, 2, 3$ and, therefore, with blade 1 moving as blade 1 of the gimbaled rotor. In both cases, the wing/pylon motion is that described in Eqs. (24) and (25). The initial time interval of the lift evolution obtained from the two configurations through the ROM approach is depicted in Fig. 15. This shows that, while the loads on blade 1 are almost identical (as expected, due to the motion identity), blades 2 and 3 experience quite different loads in the two cases that, therefore, would give rise to different aeroelastic behaviors of the wing/proprotor system.

Conclusions

A periodic-coefficient ROM for the prediction of unsteady aerodynamic loads arising on tiltrotor propellers perturbed from airplane-mode cruise flight conditions has been presented. It is a state-space model that is based on an approximation of a frequency-domain aerodynamic solution. Such a state-space model is very well suited for control applications and would be quite useful in other applications that need a simple but accurate aerodynamic model (e.g., preliminary design). The frequency-domain solution is approximated through rational matrix expressions of the aerodynamic transfer functions and, therefore, the ROM description requires the inclusion of some aerodynamic states to be added to the kinetic degrees of freedom. In this paper, the frequency-domain aerodynamic solution has been obtained by a BEM approach validated in the past for hovering and advancing rotor configurations. However, the procedure described for determining the ROM is general and applicable for whatever frequency-domain solution is available.

In the numerical investigation for the assessment of ROM accuracy, a three-bladed pylon/proprotor system with bending blades and pylon fixed to the tip section of a flapping and twisting wing has been examined. Aerodynamic loads arising both from harmonic and damped oscillatory perturbations of the wing/pylon/proprotor system have been calculated. Using the results from a time-marching (exact) BEM solution as comparison, the ROM presented here has demonstrated to be capable of predicting the loads induced by both types of perturbations with excellent accuracy. In addition, the numerical investigation has also shown that the accuracy of the aerodynamic ROM remains satisfactory if the rational approximation of the aerodynamic transfer functions is based on a number of poles considerably reduced with respect to those of the optimal solution. This implies that simplified versions of this aerodynamic ROM give reliable predictions, and this is extremely useful from the preliminary-design and control-synthesis points of view.

Appendix: BEM for Frequency-Domain Potential Aerodynamics

Consider a lifting body moving in an inviscid, incompressible flow. For $\boldsymbol{v}_f$ denoting the velocity of the fluid particles, the introduction of the potential function ϕ yields $\boldsymbol{v}_f = \nabla\phi$. This function is governed by the following Laplace equation:

$$\nabla^2\phi = 0 \qquad \text{for} \qquad \boldsymbol{x} \quad \text{outside} \quad \mathcal{S}_B \cup \mathcal{S}_W$$

where $\mathcal{S}_B$ denotes the body surface and $\mathcal{S}_W$ denotes the wake surface (i.e., the surface formed by those fluid points that have come in contact with the body surface and have left it at the trailing edge).[12] The differential problem is completed by the introduction of boundary conditions on body and wake surfaces. Following Ref. 12, in terms of potential we have $\partial\phi/\partial n = \boldsymbol{v}_B \cdot \boldsymbol{n}$ on $\mathcal{S}_B$ (with $\boldsymbol{v}_B$ denoting body velocity and $\boldsymbol{n}$ denoting the body outward unit normal), and $\Delta(\partial\phi/\partial n) = 0$ on $\mathcal{S}_W$, with $\Delta\phi = \text{const}$ following a wake material point (Δ denotes jump across the wake).

Starting from this differential formulation and applying the boundary integral equation technique, for lifting-body configurations with the wake surface fixed with respect to a body-fixed frame of reference (as it occurs, for instance, in translating wings, hovering rotors, and propellers in axial motion), it is possible to derive the following frequency-domain, incompressible-flow potential solution for $\boldsymbol{x}_* \in \mathcal{S}_B$ (see Refs. 12 and 20 for further details):

$$\frac{1}{2}\tilde{\phi}(\boldsymbol{x}_*) = \int_{\mathcal{S}_B}\left(\frac{\partial\tilde{\phi}}{\partial n}G - \tilde{\phi}\frac{\partial G}{\partial n}\right)\mathrm{d}\mathcal{S}(\boldsymbol{x}) - \int_{\mathcal{S}_W}\Delta\tilde{\phi}^{TE}e^{-s\tau}\frac{\partial G}{\partial n}\,\mathrm{d}\mathcal{S}(\boldsymbol{x}) \tag{A1}$$

In Eq. (A1), $G = -1/4\pi\|\boldsymbol{x} - \boldsymbol{x}_*\|$ is the unit source solution of the Laplace equation, whereas τ is the time necessary to convect the material wake point from the trailing edge to the current position. Note that, for configurations where the wake surface is not fixed with respect to the body-fixed frame of reference, the frequency-domain integral Eq. (A1) would not be achievable in that frequency convolution integrals would appear in the description of wake contribution.

BEM Formulation

The numerical solution of Eq. (A1) is evaluated from its algebraic approximation. It is derived by discretizing the body surface

into N_B quadrilateral panels and the wake surface into N_W quadrilateral panels. Assuming ϕ, $\partial\phi/\partial n$, and $\Delta\phi$ constant over each panel (i.e., using a zeroth-order BEM) and satisfying Eq. (A1) at the $N_c = N_B$ centers of the panels (collocation points) yields the following algebraic approximation (see Ref. 20 for details):

$$\frac{1}{2}\tilde{\phi}_k = \sum_{j=1}^{N_B} B_{kj}\tilde{\chi}_j + \sum_{j=1}^{N_B} C_{kj}\tilde{\phi}_j + \sum_{n=1}^{N_W} F_{kn}\Delta\tilde{\phi}_n^{\mathrm{TE}} \tag{A2}$$

with

$$\chi_j = \left.\frac{\partial\phi}{\partial n}\right|_{\boldsymbol{x}=\boldsymbol{x}_j} = \boldsymbol{v}_B\cdot\boldsymbol{n}|_{\boldsymbol{x}=\boldsymbol{x}_j}, \quad \phi_j = \phi(\boldsymbol{x}_j), \quad \Delta\phi_n^{\mathrm{TE}} = \Delta\phi\left(\boldsymbol{x}_n^{\mathrm{TE}}\right)$$

where $\boldsymbol{x}_j$ is the jth collocation point and $\boldsymbol{x}_n^{\mathrm{TE}}$ is the trailing-edge point from which the wake point at the center of the nth wake panel emanated. The coefficients appearing in Eq. (A2) are given by

$$B_{kj} = \int_{\mathcal{S}_{B_j}} G_k\,\mathrm{d}\mathcal{S}, \qquad C_{kj} = -\int_{\mathcal{S}_{B_j}} \frac{\partial G_k}{\partial n}\,\mathrm{d}\mathcal{S}$$

$$F_{kn} = -e^{-s\tau_n}\int_{\mathcal{S}_{W_n}} \frac{\partial \boldsymbol{G}_k}{\partial n}\,\mathrm{d}\mathcal{S}$$

where $G_k = G|_{\boldsymbol{x}_*=\boldsymbol{x}_k}$, and $\mathcal{S}_{B\,j}$ and $\mathcal{S}_{W\,n}$ denote the surfaces of the jth panel of $\mathcal{S}_B$ and of the nth panel of $\mathcal{S}_W$, respectively.

Finally, expressing the potential discontinuity $\Delta\phi_n^{\mathrm{TE}}$ in terms of the values of potential at the center of the corresponding trailing-edge panel, Eq. (A2) may be recast in the following matrix form:

$$\tilde{\underline{\phi}} = \underline{E}_{\phi}(s)\,\tilde{\underline{\chi}} \tag{A3}$$

where $\underline{\phi}$ is the column matrix collecting the ϕ_js, $\underline{\chi}$ is the column matrix collecting the χ_js, and $\underline{E}_{\phi}$ is a $[N_c \times N_c]$ matrix given by

$$\underline{E}_{\phi}(s) = \left[\tfrac{1}{2}\underline{I} - \underline{C} - \underline{F}(s)\underline{S}\right]^{-1}\underline{B} \tag{A4}$$

where $\underline{S}$ denotes the matrix that relates potential discontinuity on the wake with potential at the trailing edge.

Generalized Aerodynamic Forces

Once the potential distribution over the lifting body has been evaluated, the application of the Bernoulli theorem yields the pressure distribution and, through integration, the generalized aerodynamic forces.

In a frame of reference connected with the body, the Bernoulli theorem has the form

$$\frac{\partial\phi}{\partial t} - \boldsymbol{v}_B\cdot\nabla\phi + \frac{\|\boldsymbol{v}_f\|^2}{2} + \frac{p}{\rho} = \frac{p_\infty}{\rho} \tag{A5}$$

where p denotes local pressure, p_∞ is the pressure of the undisturbed flow, ρ denotes air density, and $\partial/\partial t$ denotes time derivative in a fixed-blade frame. Letting ϕ_0 and p_0 denote, respectively, the velocity potential and the corresponding pressure field around the body in its reference configuration (reference aerodynamic solution), and letting φ and p' denote, respectively, velocity potential and pressure field produced by perturbation motion, then one has $\phi = \phi_0 + \varphi$ and $p = p_0 + p'$. Substituting these expressions into Eq. (A5), dropping reference-state and second-order perturbative terms, and transforming into frequency domain yields the following linearized expression for the pressure perturbation:

$$\tilde{p}' = -\rho[s\tilde{\varphi} + (\nabla\phi_0 - \boldsymbol{v}_B)\cdot\nabla\tilde{\varphi}] \tag{A6}$$

Using the body panel discretization introduced earlier, and expressing $\nabla\tilde{\varphi}$ through the potential evaluated at the blade collocation points, Eq. (A6) may be recast in the following matrix form:

$$\tilde{\underline{p}}' = \underline{E}_p(s)\,\tilde{\underline{\varphi}} \tag{A7}$$

where $\underline{p}'$ and $\underline{\varphi}$ are column matrices that collect the values of the perturbation pressure and of the perturbation potential at the collocation points, respectively.

Then the generalized perturbation forces are defined through the following expression:

$$f_n = -\int_{\mathcal{S}_B} p'\boldsymbol{n}\cdot\boldsymbol{\Upsilon}_n(\boldsymbol{x})\,\mathrm{d}\mathcal{S}(\boldsymbol{x})$$

where $\boldsymbol{\Upsilon}_n$ are a set of N_f vector shape functions with time-constant components in a frame of reference connected with the undeformed body. Note that, for aeroelastic analysis, this set of shape functions has to coincide with that used for defining the body rigid and elastic motion [i.e., with the shape functions appearing in Eqs. (3) and (15), in our case]. Then, considering again the body surface discretization applied in the BEM formulation, the following matrix relationship may be obtained in the frequency domain:

$$\tilde{\underline{f}} = \underline{E}_f\,\tilde{\underline{p}}' \tag{A8}$$

where the entries of the $[N_f \times N_c]$ matrix $\boldsymbol{E}_f$ are defined as

$$E_{f_{nj}} = -\int_{\mathcal{S}_{B\,j}} \boldsymbol{n}\cdot\boldsymbol{\Upsilon}_n(\boldsymbol{x})\,\mathrm{d}\mathcal{S}(\boldsymbol{x})$$

with $\mathcal{S}_{B\,j}$ denoting the surface of the jth body panel.

Finally, combining Eq. (A3) (written for perturbative variables) with Eqs. (A7) and (A8) yields the following linear relationship between boundary conditions and generalized aerodynamic forces associated with a small-perturbation motion of the body:

$$\tilde{\underline{f}} = \underline{Q}(s)\,\tilde{\underline{\chi}} \tag{A9}$$

where the $[N_f \times N_c]$ matrix $\underline{Q}$ is given by

$$\underline{Q}(s) = \underline{E}_f\,\underline{E}_p(s)\,\underline{E}_{\phi}(s) \tag{A10}$$

References

[1]Johnson, W., "Dynamics of Tilting Proprotor Aircraft in Cruise Flight," NASA TN D-7677, May 1974.

[2]Nixon, M. W., "Aeroelastic Response and Stability of Tiltrotors with Elastically-Coupled Composite Rotor Blades," Ph.D. Dissertation, Dept. of Aerospace Engineering, University of Maryland, College Park, MD, 1993.

[3]Srinivas, V., Chopra, I., and Nixon, M. W.,"Aeroelastic Analysis of Advanced Geometry Tiltrotor Aircraft," *Journal of the American Helicopter Society*, Vol. 43, No. 3, 1998, pp. 212–221.

[4]Srinivas, V., and Chopra, I., "Validation of a Comprehensive Aeroelastic Analysis for Tiltrotor Aircraft," *Journal of the American Helicopter Society*, Vol. 43, No. 4, 1998, pp. 333–341.

[5]Nixon, M. W., Piatak, D. J., Corso, L. M., and Popelka, D. A., "Aeroelastic Tailoring for Stability Augmentation and Performance Enhancements of Tiltrotor Aircraft," *Journal of the American Helicopter Society*, Vol. 45, No. 4, 2000, pp. 270–279.

[6]Singh, B., and Chopra, I.,"Whirl Flutter Stability of Two-Bladed Proprotor/Pylon System in High Speed Flight," *Journal of the American Helicopter Society*, Vol. 48, No. 2, 2003, pp. 99–107.

[7]Kunz, D. L., "Analysis of Prop-Rotor Whirl Flutter: Review and Update," AIAA Paper 2002-1602, April 2002.

[8]Nitzsche, F.,"Whirl-Flutter Suppression in Advanced Turboprop and Propfans by Active Control Techniques," *Journal of Aircraft*, Vol. 31, No. 3, 1994, pp. 713–719.

[9]Gaonkar, G. H., and Peters, D. A., "Review of Dynamic Inflow Modeling for Rotorcraft Flight Dynamics," *Vertica*, Vol. 12, No. 3, 1988, pp. 213–242.

[10]Peters, D. A., and He, C. J., "Finite-State Induced Flow Models, Part II: Three-Dimensional Rotor Disk," *Journal of Aircraft*, Vol. 32, No. 2, 1995, pp. 323–333.

[11]Stettner, M., Schrage, D. P., and Peters, D. A., "Application of a State-Space Wake Model to Tiltrotor Wing Unsteady Aerodynamics," *Proceedings of the American Helicopter Society Aeromechanics Specialists Conference*, American Helicopter Society, Alexandria, VA, Jan. 1994.

[12]Morino, L., and Gennaretti, M., "Boundary Integral Equation Methods for Aerodynamics," *Computational Nonlinear Mechanics in Aerospace Engineering*, edited by S. N. Atluri, Progress in Astronautics and Aeronautics, Vol. 146, AIAA, New York, 1992, pp. 279–320.

[13]Gennaretti, M., Luceri, L., and Morino, L., "A Unified Boundary Integral Methodology for Aerodynamics and Aeroacoustics of Rotors," *Journal of Sound and Vibration*, Vol. 200, No. 4, 1997, pp. 467–489.

[14]Karpel, M., "Design for the Active Flutter Suppression and Gust Alleviation Using State-Space Aeroelastic Modeling," *Journal of Aircraft*, Vol. 19, No. 3, 1982, pp. 221–227.

[15]Hoadley, S. T., and Karpel, M., "Application of Aeroservoelastic Modeling Using Minimum-State Unsteady Aerodynamic Approximations," *Journal of Guidance, Control, and Dynamics*, Vol. 14, No. 6, 1991, pp. 1267–1276.

[16]Morino, L., Mastroddi, F., De Troia, R., Ghiringhelli, G. L., and Mantegazza, P., "Matrix Fraction Approach for Finite-State Aerodynamic Modeling," *AIAA Journal*, Vol. 33, No. 4, 1995, pp. 703–711.

[17]Gennaretti, M., and Ponzi, C., "Finite-State Aerodynamic Modelling for Gust Load Alleviation of Wing-Tail Configurations," *Aeronautical Journal*, Vol. 103, No. 1021, 1999, pp. 147–158.

[18]Gennaretti, M., and Lisandrin, P., "Flap-Lag Rotor Dynamics and Aeroelastic Stability Using Finite-State Aerodynamics," *Proceedings of the 24th European Rotorcraft Forum*, Association Aéronautique et Astronautique de France, Marseilles, France, Sept. 1998, pp. DY.01.1–DY.01.11.

[19]Gennaretti, M., and Iemma, U., "Aeroacoustoelasticity in State-Space Format Using CHIEF regularization," *Journal of Fluids and Structures*, Vol. 17, No. 7, 2003, pp. 983–999.

[20]Morino, L., "A General Theory of Unsteady, Compressible, Potential Aerodynamics," NASA CR-2464, Dec. 1974.